mater.scichina.com link.springer.com

Published online 30 November 2022 | https://doi.org/10.1007/s40843-022-2247-0
Sci China Mater 2023, 66(4): 1417–1426

Size-engineered noble metal nanoclusters synthesized by impregnation for size-dependent catalysis

Zhibin Wen, Shumeng Zhang, Zhaojun Liu, Zhixue Zhang, Zhun Qiao, Kai Liu and Chuanbo Gao*

ABSTRACT Noble metal nanoclusters, as a bridge between atoms and nanoparticles, show extraordinary catalytic activities because of their unique electronic structures. Such nanoclusters are usually synthesized by a wet chemical approach through unfavorable surface passivation by ligands and have not been obtained by an impregnation approach with satisfactory size uniformity. Herein, we report highly uniform ligand-free noble metal nanoclusters, such as Pd nanoclusters, synthesized each in a silica capsule by an impregnation strategy, with their size accurately engineerable in the range of 0.9–2.9 nm. The key is to ensure the impregnation synthesis with strict control over the nucleation and growth of noble metal nanoclusters by involving hollow silica nanoreactors and non-noble metal competitor ions, thereby showing unprecedented advantages of operational simplicity, scalability, and excellent size controllability. These Pd nanoclusters exhibit a strong size effect on catalysis exemplified by the alcohol oxidation-Knoevenagel condensation sequential reaction, with those of 1.3 nm exhibiting the highest catalytic activity. We believe this novel strategy opens new opportunities for rationally designing efficient noble metal nanocluster-type catalysts for a broad range of important reactions and bringing laboratory-quality nanoclusters into large-scale applications.

Keywords: noble metal nanoclusters, ligand-free, size engineering, impregnation synthesis, size-dependent catalysis

INTRODUCTION

Noble metal nanoclusters with typical sizes from subnanometer to approximately 2 nm have emerged as an important family of catalysts, which may have a strong impact on a broad range of catalytic applications [1–11]. As a bridge between atoms and nanoparticles, metal nanoclusters show unique electronic band structures and, therefore, catalytic properties different from noble metal nanoparticles with large sizes [6–11]. Moreover, the metal atoms in these nanoclusters are primarily located on the surface with rich corner and edge sites because of their ultrasmall size [11]. Both may make a substantial change to the way the noble metal nanoclusters interact with guest molecules, i.e., reactants and reaction intermediates in catalysis, leading to extraordinary catalytic properties. For example, Kuhn *et al.* [6] demonstrated the size-dependent catalytic selectivity of Pt nanoclusters in a pyrrole hydrogenation reaction. Liu *et al.* [12], Li and Jin [13], and Li *et al.* [14] reported size-dependent catalytic activities of Au nanoclusters in an organic oxidation reaction and a hydrogenation reaction. Our group also determined that Pt nanoclusters of 1.7 nm are particularly active for the hydrogenation of quinoline and thus superior to large-sized nanoparticles [8,15,16]. To date, great efforts have been devoted to the controlled wet chemical colloidal synthesis of noble metal nanoclusters. Currently, atomically precise metal nanoclusters can be synthesized using strong thiolated capping ligands [1,17–19]. Metal nanoclusters can also be obtained through confined synthesis within dendrimers [20–22], molecular cages [23–27], and reverse micelles [16,28,29]. However, thiolate and other organic ligands in colloidal synthesis significantly passivate the metal surface, making it difficult to fully expose the active sites [30–33]. Moreover, colloidal synthesis is usually difficult to scale up for large-scale applications. Therefore, the synthesis of size-engineered ligand-free noble metal nanoclusters with scale-up capability for practical applications remains a great challenge.

Compared with controlled wet chemical colloidal synthesis, impregnation synthesis is a more prevalent strategy for preparing surface-clean noble metal catalysts for industrial applications because of its simplicity and scalability for mass production [34–36]. Although noble metal nanoclusters can also form *via* impregnation synthesis, the synthesis often produces a mixture of metal nanoclusters and particles with a broad size distribution because of the lack of control over particle nucleation and growth. On the one hand, noble metal ions are prone to adsorbing onto the support along their diffuse paths during the impregnation process, causing local concentration variations [34]. Therefore, nucleation events occur at high-concentration sites that are randomly distributed on the support. On the other hand, noble metal nanoclusters and particles grow on a continuous surface of the support without clear boundaries to define the noble metal supplies for a specific nucleus. Consequently, the growth of nuclei is influenced by the local availability of noble metal ions, leading to a broad size distribution [34–36]. In this sense, introducing a confined space is beneficial for the controlled synthesis of metal nanoclusters [37,38]. The ideal synthesis should follow an impregnation process for simplicity and scalability but strictly control the nucleation and growth of noble metal nanoclusters for accurate size engineering in a manner resembling the laboratory colloidal synthesis, thus possessing the potential to bring laboratory-quality noble metal nanoclusters into industrial applications, which, however, is yet to be established.

Frontier Institute of Science and Technology, Xi'an Jiaotong University, Xi'an 710054, China
* Corresponding author (email: gaochuanbo@mail.xjtu.edu.cn)

Herein, we report highly uniform ligand-free noble metal nanoclusters synthesized, each in a silica capsule, by an impregnation paradigm, showing combined advantages of operational simplicity, scalability, and excellent size controllability in the range of subnanometer to 2.9 nm. The key is to introduce non-noble metal "competitor ions" into inorganic nanoreactor-based synthesis. The competitor ions, e.g., Cu^{2+}, have been proven successful in homogenizing the adsorption of noble metal ions inside inorganic nanoreactors, thus ensuring only one nucleation event in each nanoreactor upon reduction. The nanoreactors (i.e., hollow silica nanorods) define the boundaries of the metal supply for nucleus growth, thus restraining the growth extent of noble metal nanoclusters to designable ultrasmall sizes. Through these means, both the nucleation and growth of noble metal nanoclusters become strictly controlled without sacrificing the simplicity of the impregnation operation. This synthesis guarantees exceptional synthetic accuracy at the nanoscale: only one noble metal nanocluster (Pd for demonstration) exists in an individual hollow silica nanorod, with the size accurately tunable in the range of 0.9–2.9 nm (size uncertainty of approximately 0.2 nm). The accurate size engineering, as well as the clean surface, enables us not only to achieve exceptional catalytic activities but also to unambiguously reveal their dependence on the size of the nanoclusters in a broad range of reactions, as demonstrated in this study by the alcohol oxidation-Knoevenagel condensation sequential reaction. Pd nanoclusters of 1.3 nm exhibit high catalytic activity, superior to Pd nanoclusters of 0.9, 1.8, 2.2, and 2.9 nm. We believe the size-engineered ligand-free noble metal nanoclusters can be applied to a broader range of important catalytic processes, which holds promise to achieve significantly enhanced catalytic performance because of the drastically different electronic properties of the nanoclusters in the specific size range.

EXPERIMENTAL SECTION

Synthesis of hollow silica nanorods

Hollow silica nanorods were synthesized by following our previous protocol [39,40]. Typically, 8.5 g of polyoxyethylene(10) cetyl ether (Brij C10) was dissolved in 15 mL of cyclohexane at 50°C. Subsequently, 0.9 mL of $NiCl_2$ (0.8 mol L^{-1}) was added to the solution and stirred until homogeneity was achieved. Thereafter, 0.45 mL of hydrazine hydrate ($N_2H_4{\cdot}H_2O$) was added dropwise and stirred for 3 h to form nickel-hydrazine complex nanorods. To the synthesis system, 50 μL of (3-aminopropyl)-triethxoysilane and 1 mL of diethylamine were added, and 1.5 h later, 1 mL of tetraethyl orthosilicate was added. After stirring for another 3 h, nickel-hydrazine@SiO_2 core-shell nanorods were collected by centrifugation. The nickel-hydrazine complex was etched *via* refluxing in 1 mol L^{-1} of HCl in ethanol for 12 h. Hollow silica nanorods were collected through centrifugation, deprotonated using $NH_3{\cdot}H_2O$, washed using ethanol/H_2O, and dried at 60°C to form a powder for future use.

Synthesis of Pd-*x*@SiO_2

Pd nanoclusters were synthesized in hollow silica nanorods by a modified impregnation method. In a typical synthesis, 0.5 g of hollow silica nanorods was mixed with 5 mL of $CuCl_2$ (40 mmol L^{-1}) and 5 mL of H_2PdCl_4 (4 mmol L^{-1}). The solid was recovered through centrifugation and washed with H_2O. Subsequently, the solid was mixed with 10 mL of ascorbic acid (10 mmol L^{-1}) to yield Pd nanoclusters (average size of approximately 1.3 nm). The size of the Pd nanoclusters was tuned by adjusting the Pd^{2+}/Cu^{2+} ratio in the precursor (Table S1). The Pd-*x*@SiO_2 nanorods were etched using water to form nanopores to facilitate the mass transfer. Typically, 0.5 g of Pd-*x*@SiO_2 was added to 100 mL of H_2O and heated at 80°C for 2 h. The solid was recovered through centrifugation and dried in air.

Synthesis of Au, Pt, and Ru@SiO_2

Au, Pt, and Ru@SiO_2 nanorods were synthesized by following a similar procedure with a metal salt of $HAuCl_4$, H_2PtCl_6, or $RuCl_3$ in place of H_2PdCl_4. Moreover, 10 mL of $NaBH_4$ (10 mmol L^{-1}) was used as the reducing agent in place of 10 mL of ascorbic acid (10 mmol L^{-1}) for the synthesis of Ru@SiO_2 to overcome the low reduction potential of Ru^{3+}.

Alcohol oxidation-Knoevenagel condensation sequential catalysis

In typical catalysis, 0.5 mmol of benzyl alcohol, 0.6 mmol of malononitrile, and the Pd-*x*@SiO_2 catalyst (Pd, 0.025 mol% of benzyl alcohol) were added to a mixed solvent of methanol (1 mL) and *N*,*N*-dimethylformamide (1 mL). The mixture was stirred in ambient air at room temperature (25°C). After the reaction, aliquots of the mixture were diluted using methanol and analyzed by gas chromatography-mass spectrometry.

^{1}H NMR analysis of the surface-bound organic molecules on Pd nanoclusters

To obtain the ^{1}H nuclear magnetic resonance (NMR) spectra of the Pd-*x*@SiO_2 (x = 0.9, 1.3, 1.8, 2.2, and 2.9 nm) catalysts with surface-bound benzyl alcohol and benzaldehyde, 50 mg of the Pd-*x*@SiO_2 catalyst was mixed with 0.1 mmol of benzyl alcohol (or benzaldehyde). Subsequently, the samples were repetitively washed (four times) using $CDCl_3$ to remove free benzyl alcohol and benzaldehyde molecules and redispersed in $CDCl_3$ for NMR analysis.

RESULTS AND DISCUSSION

Design of the synthesis

We aim to endow the impregnation synthesis of noble metal nanoclusters with accurate size engineering, thus imparting the nanoclusters with high quality comparable to the quality of those obtained through colloidal synthesis. For this purpose, impregnation synthesis should be redesigned to reliably overcome the uncontrollability in both the nucleation and growth of noble metal nanoclusters. The growth extent of metal nanoclusters is controlled by dividing the continuous surface of the support in conventional impregnation synthesis (Scheme 1, route a) into discrete ones with definite boundaries. To this end, we introduce hollow silica nanorods, which can be synthesized on a large scale [39], as nanoreactors (Scheme 1, route b). The interior surface of the hollow silica nanorods is selectively functionalized by amino groups, which confines the adsorption of the metal precursor inside the nanoreactors, thereby defining the boundaries of the metal supply for the growth of an individual nucleus. In this manner, the size of the metal nanoclusters becomes controllable, if a single nucleus forms in each nanoreactor. However, multiple nucleation events may occur in an individual nanoreactor because of the inhomogeneous adsorption of the metal ions in it,

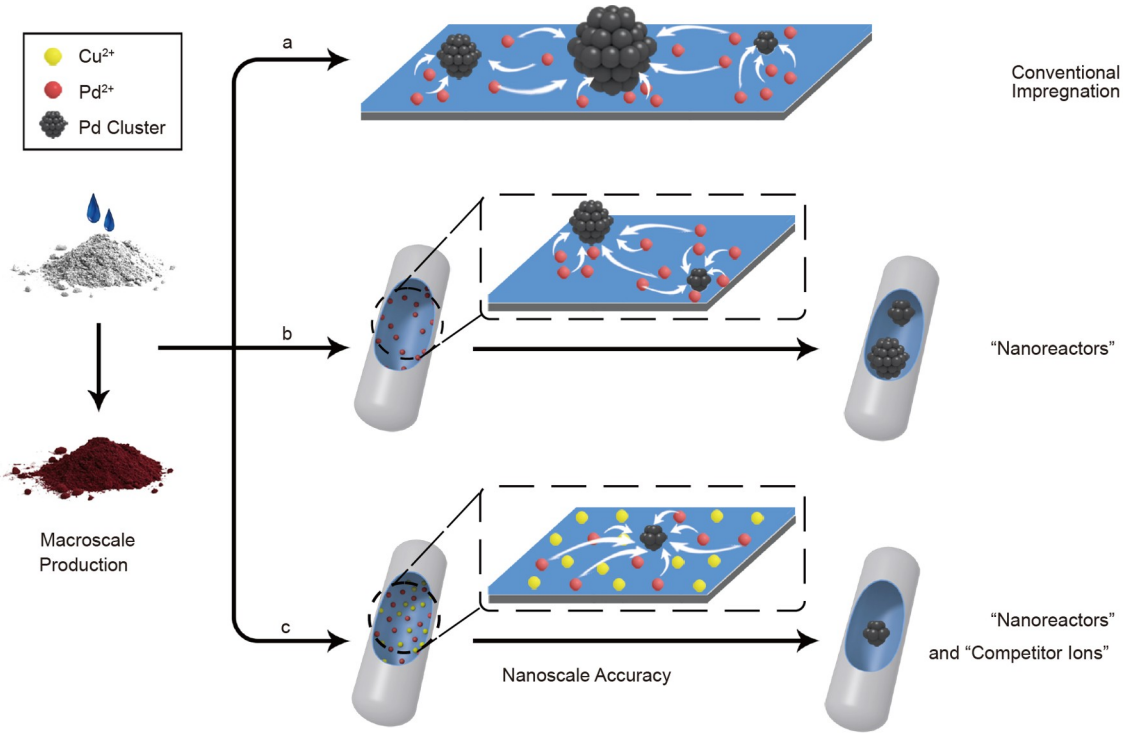

Scheme 1 Impregnation synthesis of noble metal nanoclusters.

also causing a loss of size uniformity. To suppress the multiple nucleation events in the nanoreactors, we then introduce non-noble metal ions, e.g., Cu^{2+}, as competitor ions in order that the local concentration variations of the noble metal precursors in the nanoreactors could be eliminated (Scheme 1, route c). Considering Pd^{2+} as an example, its adsorption-desorption equilibrium in a nanoreactor undergoes a shift from (1) to (2) (where * denotes the adsorption site):

$$* + Pd^{2+} \rightleftharpoons *Pd^{2+},$$

$$K_1 = [*Pd^{2+}]/[Pd^{2+}], \quad (1)$$

$$*Cu^{2+} + Pd^{2+} \rightleftharpoons Cu^{2+} + *Pd^{2+},$$

$$K_2 = ([*Pd^{2+}]/[Pd^{2+}]) \times ([Cu^{2+}])/[*Cu^{2+}]). \quad (2)$$

The equilibrium (2) is coupled with the adsorption-desorption equilibrium of Cu^{2+} (3):

$$* + Cu^{2+} \rightleftharpoons *Cu^{2+},$$

$$K_3 = [*Cu^{2+}]/[Cu^{2+}]. \quad (3)$$

Therefore, $K_2 = K_1/K_3$. In the absence of competitor ions, the adsorption-desorption equilibrium constant of Pd^{2+} (K_1) has a large value because of the strong coordination interaction between Pd^{2+} and amine groups in the nanoreactors. Therefore, Pd^{2+} ions are difficult to desorb once adsorbed, leading to inhomogeneous adsorption along their diffuse paths, which accounts for the multiple nucleation events in an individual nanoreactor. Using the competitor Cu^{2+} ions, the adsorption-desorption equilibrium constant of Pd^{2+} (K_2) becomes K_1/K_3, which has a value smaller than K_1, ideally approaching unity, indicating that the adsorption-desorption of Pd^{2+} becomes substantially reversible. In this case, the adsorption of Pd^{2+} is homogeneous after adsorption-desorption cycles, leading to the reliable elimination of multiple nucleation events in individual nanoreactors. The size of Pd nanoclusters is determined solely by the quantity of Pd^{2+} thermodynamically adsorbed in the nanoreactor, thus becoming highly controllable.

Impregnation synthesis of uniform noble metal nanoclusters

The efficacy of the experimental design for the controlled impregnation synthesis of noble metal nanoclusters can be verified by a series of control experiments. A simple impregnation synthesis (Scheme 1, route a) produces Pd nanoclusters and particles with an average size of 5.10 ± 1.51 nm (mean ± standard deviation, measured statistically from more than 100 particles, applied hereafter) on amino-functionalized silica nanospheres (Fig. 1a). The individual particle size ranges from approximately 8 nm to approximately 1 nm, showing a broad distribution because of the lack of control over the nucleation and growth of Pd on the continuous surface of the silica nanospheres. Then, we investigated the impregnation synthesis using amino-functionalized hollow silica nanorods as nanoreactors (Scheme 1, route b), leading to a reduced average particle size of 2.39 ± 1.00 nm (Fig. 1b). However, multiple Pd nanoclusters or particles are detected in each hollow silica nanorod, as expected, indicating the occurrence of multiple nucleation events in it. Therefore, although the nanoreactors can restrain the growth of Pd into ultrasmall sizes, they cannot control the nucleation of the nanoclusters, leading to poor size uniformity. The individual particle size ranges from approximately 4.5 nm to approximately 1.1 nm. Our strategy combines the concepts of "nanoreactors" and "competitor ions" (Scheme 1, route c). Using the competitor Cu^{2+} ions, only one Pd particle was formed in each hollow silica nanorod, indicating successful suppression of the multiple nucleation events in individual nanoreactors (Fig. 1c). Consequently, Pd nanoclusters with an average size of 1.46 ± 0.19 nm were obtained. The significantly small size uncertainty of approximately 0.2 nm confirms the high size uniformity of the Pd nanoclusters, verifying the synthetic accuracy of our strategy at the nanoscale, albeit with the simple impregnation operation (Fig. 1d).

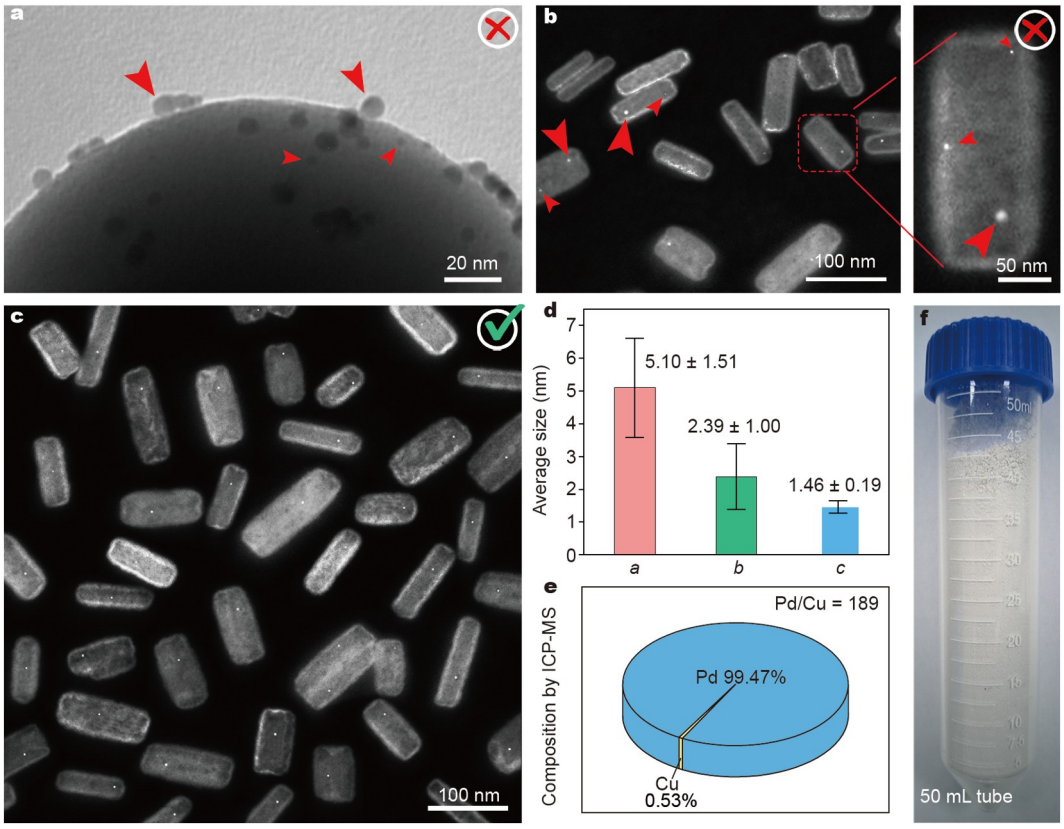

Figure 1 Pd nanoclusters synthesized through different routes: (a) transmission electron microscopy (TEM) image of Pd nanoclusters and particles on silica nanospheres synthesized by a conventional impregnation method (Scheme 1, route a). (b) High-angle annular dark-field scanning TEM (HAADF-STEM) image of Pd nanoclusters and particles in the nanoreactors of hollow silica nanorods without competitor ions in the synthesis (Scheme 1, route b). (c) HAADF-STEM image of uniform Pd nanoclusters in hollow silica nanorods with competitor Cu^{2+} ions in the synthesis (Scheme 1, route c). (d) Average sizes of the Pd nanoclusters or particles, corresponding to (a) to (c). Error bars: standard deviations. (e) Chemical composition of the Pd nanoclusters synthesized by route c, measured by ICP-MS. (f) A photograph of the product synthesized by route c in a 50-mL tube.

We further investigated the chemical composition of Pd nanoclusters *via* inductively coupled plasma mass spectrometry (ICP-MS) (Fig. 1e and Table S2). The Pd nanoclusters are composed of 99.47% Pd and 0.53% Cu, showing a high Pd/Cu ratio of 189. Thus, Cu in the Pd nanoclusters is negligible, which is a result of the inevitable but insignificant reduction of Cu^{2+} in the synthesis. Considering that an excess of Cu^{2+} was used in the synthesis, the trace amount of Cu in the nanoclusters confirms that the Cu^{2+} ions as non-noble metal competitor ions were not effectively reduced and were simply spectators during the chemical reduction, which can be explained by the large reduction potential difference of the metal ions (E^{Θ} [Cu^{2+} + $2e^{-}$ ⇌ Cu] = +0.34 V; E^{Θ} [Pd^{2+} + $2e^{-}$ ⇌ Pd] = +0.95 V) [41]. Therefore, the nanoclusters can be regarded as monometallic ones.

Because our impregnation synthesis is conducted with hollow silica nanoreactors obtainable in a large amount from a reverse micellar system [39], this strategy is readily scalable to produce a large amount of Pd nanocluster-type catalysts for practical applications. As a demonstration, 12.5 g of the catalyst (Pd nanoclusters of 1.3 nm) was obtained from a single batch starting from approximately 500 mL of a reverse micellar system for the synthesis of hollow silica nanorods. Fig. 1f shows a photograph of the catalyst (additional images are shown in Fig. S1). The powder has a gray color, which is typical for Pd nanoclusters encapsulated in silica capsules. Therefore, our impregnation synthesis can unify nanoscale accuracy and large-scale production for the synthesis of noble metal nanoclusters.

Accurate size and compositional engineering of noble metal nanoclusters

The size of the noble metal nanoclusters obtained *via* the impregnation synthesis is highly controllable (Fig. 2a and Table S1). Because the competitor Cu^{2+} ions do not participate in the growth of nanoclusters, the final size of the nanoclusters solely depends on the quantity of the Pd^{2+} ions available in each nanoreactor, i.e., the Pd^{2+}/Cu^{2+} ratio in the precursor, considering that both metal ions in excess reach a adsorption-desorption equilibrium in the nanoreactor before the reduction. Therefore, we can synthesize uniform Pd nanoclusters (average size of 0.9–2.9 nm by varying the Pd^{2+}/Cu^{2+} ratio during the synthesis; Fig. 2b–f). These catalysts are designated as Pd-x@SiO_2, where x denotes the average size of the Pd nanoclusters (unit: nm). All the samples show exclusively one Pd nanocluster in each hollow silica nanorod. The Pd nanoclusters are highly uniform with negligibly small standard deviations (additional TEM images are shown in Fig. S2). Theoretically, the volume of an individual Pd nanocluster represented by d^3 (where d is the size of the nanocluster) is proportional to $n_{Pd}/(n_{Pd} + n_{Cu})$ (where n is the quantity of the metal precursors), assuming saturated adsorption of the binary metal ions in the nanoreactors. By plotting the data, we can establish the relationship $d^3 = 25.67n_{Pd}/(n_{Pd} + n_{Cu})$ with a correlation coefficient (r^2) of

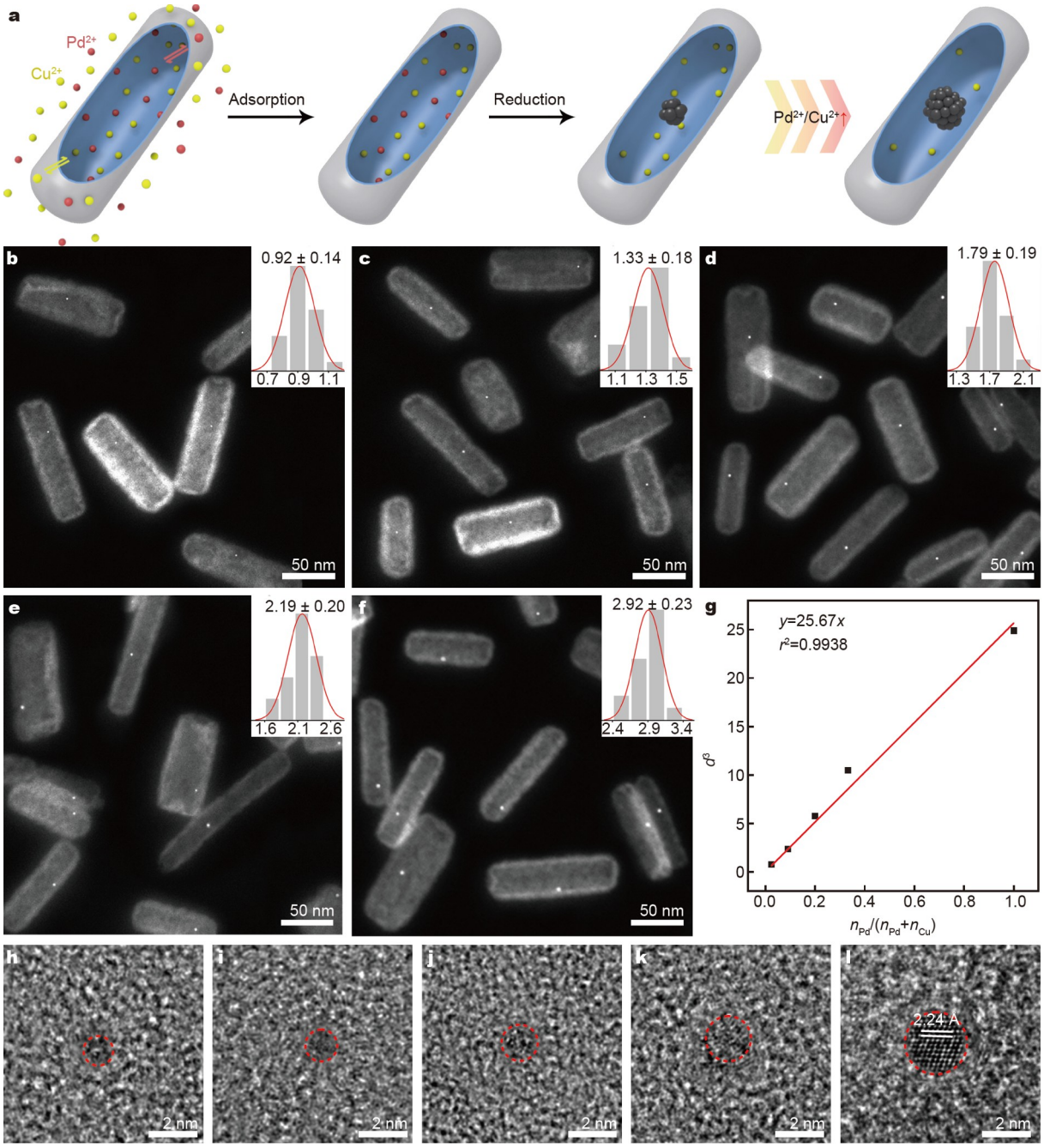

Figure 2 Size engineering of Pd nanoclusters in hollow silica nanorods: (a) mechanism for the accurate size control of the nanocluster by the Pd^{2+}/Cu^{2+} ratio in the precursor. (b–f) HAADF-STEM images of Pd-x@SiO_2 (x = 0.9, 1.3, 1.8, 2.2, and 2.9 nm) after H_2O etching. The inset shows the size distributions of the Pd nanoclusters (unit: nm). The average sizes are expressed as the "mean ± standard deviation". (g) Volume of the Pd nanoclusters (using average sizes) as a function of the molar fractions of Pd^{2+} in the metal precursors. (h–l) High-resolution TEM images of the Pd nanoclusters with different sizes. From left to right: 0.9, 1.3, 1.8, 2.2, and 2.9 nm. The red circles outline the contours of the Pd nanoclusters.

0.9938, which well verifies our hypothesis (Fig. 2g). Therefore, the ultrasmall size of Pd nanoclusters becomes accurately predictable according to the precursors of the synthesis. Fig. 2h–l show the high-resolution TEM images of the Pd nanoclusters. Regular lattices can be observed in Pd nanoclusters of 2.9 nm, corresponding to a face-centered cubic phase. When the size decreases to the nanocluster region, the lattice is less discernible and eventually disappears, indicating the transformation of the structure from crystalline to amorphous, consistent with previous reports [8,42,43].

The Pd nanoclusters show size-dependent oxidation states, as revealed by the core-level Pd 3d X-ray photoelectron spectroscopy (XPS) (Fig. 3a) [8]. When the Pd size is within the range of 1.8–2.9 nm, the Pd 3d XPS can be fitted by Pd(0) and Pd(II) components. With the decrease in size, the intensity of the Pd(0) peaks decreases, whereas that of the Pd(II) peak increases, indicating the increasing oxidation state of the Pd nanoclusters. When the size of the Pd nanoclusters decreases to 1.3 nm, the Pd(IV) peaks emerge, whereas the Pd(0) peaks disappear, showing the characteristics of an oxide, which indicates an even

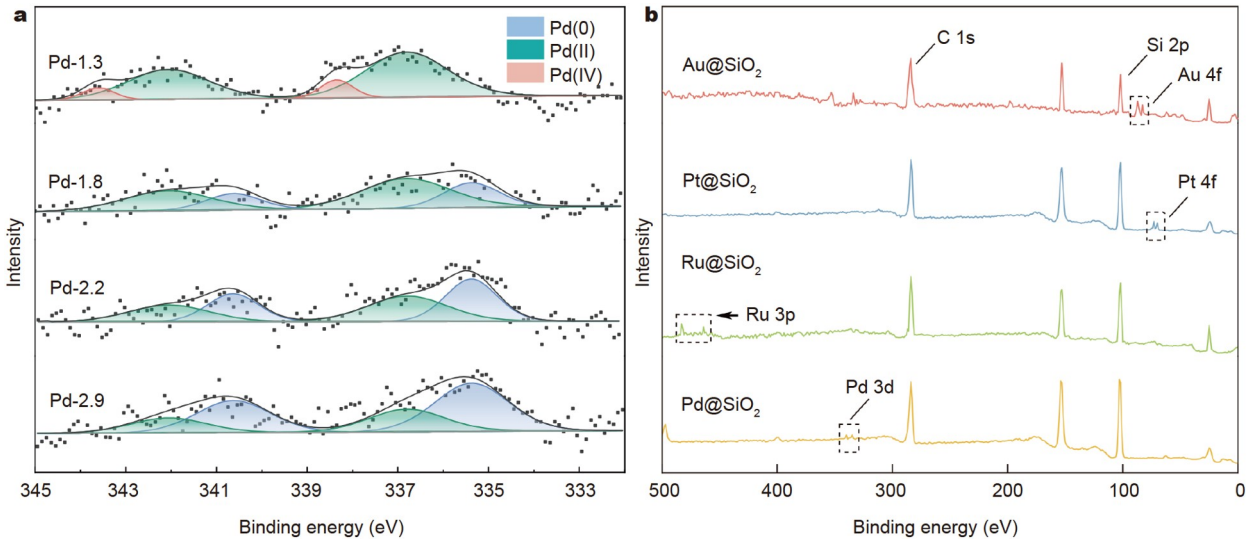

Figure 3 XPS of the noble metal nanoclusters in hollow silica nanorods. (a) Core-level Pd 3d XPS of the Pd-*x*@SiO_2 catalysts. (b) XPS of Au, Pt, Ru, and Pd nanoclusters in hollow silica nanorods.

elevated oxidation state of the Pd nanoclusters. The oxidation state transition can be attributed to the high reactivity of Pd nanoclusters with an ultrasmall size, leading to their oxidation when exposed to ambient air. The size-dependent electronic properties of the Pd nanoclusters may have a pronounced influence on their catalytic properties.

This strategy is generally applicable to the synthesis of a broad range of noble metal nanoclusters in hollow silica nanorods. To demonstrate it, we successfully prepared Au@SiO_2, Pt@SiO_2, and Ru@SiO_2 catalysts by simply replacing H_2PdCl_4 with $HAuCl_4$, H_2PtCl_6, and $RuCl_3$ in the impregnation synthesis. The core-level XPS peaks of the corresponding metals are distinct (Fig. 3b). TEM images show that the structures of the catalysts are similar to that of the Pd@SiO_2 catalyst (Fig. S3). For all the samples, only a single metal nanocluster is formed in each hollow silica nanorod, and the metal nanoclusters are highly uniform, which confirms the high-level control of this strategy regardless of the types of noble metals.

Size-dependent catalytic properties of Pd nanocluster@SiO_2 catalysts

Noble metal nanoclusters in hollow silica nanorods show clear advantages over conventional catalysts. First, the noble metal nanoclusters are ligand-free; therefore, their surfaces can be fully exposed to the reactants. Second, the size of the noble metal nanoclusters is accurately tunable, which enables the identification of the active sites for catalysis. Third, the nanoreactors provide a manageable local environment for the noble metal nanoclusters, which may profoundly influence their catalytic properties. Finally, the nanoclusters are encapsulated in hollow silica nanorods and thus are highly stable against agglomeration [2]. Notably, nanopores can be created in the silica nanorods through etching using water, which facilitates the mass transfer across the silica layers (Figs S4 and S5) [44]. To take full advantage of these merits, we demonstrate the application of the Pd-*x*@SiO_2 catalysts (x = 0.9, 1.3, 1.8, 2.2, and 2.9 nm) in the alcohol oxidation-Knoevenagel condensation sequential reaction (Fig. 4a) [45–47]. Benzyl alcohol is first oxidized to an intermediate of benzaldehyde by ambient air and then condensed with malononitrile to yield benzylidene malononitrile. The alcohol oxidation and sequential condensation reactions occur on the Pd nanoclusters and basic amino sites, respectively, making the Pd/–NH_2 interface the active site for catalysis. More details about the conditions and scope of the reaction are provided in the Supplementary information (Tables S3 and S4).

The Pd nanoclusters show size-dependent catalytic activities in the sequential reaction (Fig. 4b). Among all sizes investigated (i.e., 0.9–2.9 nm), the nanoclusters of 1.3 nm showed the highest activity. The conversion of benzyl alcohol reached >99% within 8 h. To better reveal the size effect of the Pd nanoclusters on catalytic activity, we calculated the turnover frequencies (TOFs) by normalizing the activity to the number of Pd atoms on the surface (Fig. 4c; the calculation details are listed in Table S5). With the decrease in the size of the Pd nanoclusters, the TOFs first increased and then decreased, showing a volcanic shape peaking at the cluster size of 1.3 nm. The mass activity of the 1.3-nm Pd nanoclusters was also the highest among all sizes investigated, making them the most economical catalyst for this reaction (Fig. 4c). Notably, without the strong capping ligand on the surface, the Pd nanoclusters exist in the form of an oxide or hydroxide when their sizes are no larger than 1.3 nm. Control experiments show that $Pd(OH)_2$ is not an active catalyst for this reaction, which rules out the contribution of the oxidation states of Pd to the high catalytic activity of the 1.3-nm Pd nanoclusters (Fig. S6). The size dependence of the Pd nanoclusters in catalyzing the sequential reaction indicates that the alcohol oxidation reaction on the Pd nanoclusters is the rate-limiting step. Therefore, we expect and experimentally verify a strong size effect of the Pd nanoclusters in catalyzing the benzyl alcohol oxidation reaction (Fig. S7). The Pd-1.3@SiO_2 catalyst showed the highest activity among all sizes investigated, substantially exceeding the best results in the literature [48–52], which accounts for the superior activity in the overall sequential reaction.

The size effect can be attributed to the size-dependent electronic structure of the Pd nanoclusters and consequently their size-dependent interactions with reactants and intermediates [53]. To verify this, we examined the binding affinity of the key

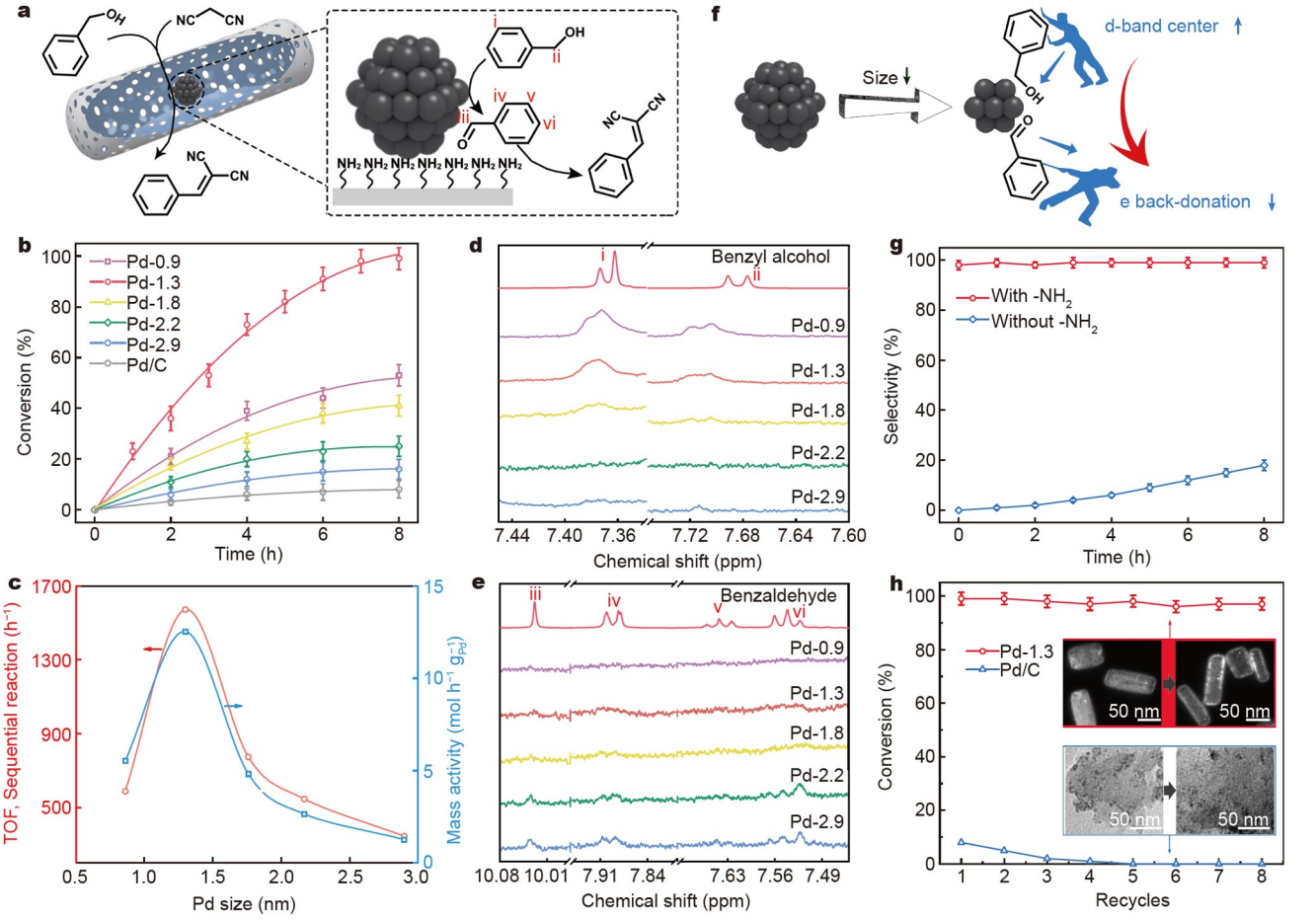

Figure 4 Catalytic properties of the Pd-*x*@SiO_2 (*x* = 0.9, 1.3, 1.8, 2.2, and 2.9 nm) catalysts in the alcohol oxidation-Knoevenagel condensation sequential reaction: (a) scheme of the reaction at the Pd/–NH_2 interface in the hollow silica nanoreactors. (b) Plots of benzyl alcohol conversion *versus* the reaction time. (c) Plots of TOFs and mass activities *versus* the size of the Pd nanoclusters. ^{1}H NMR spectra of (d) benzyl alcohol and (e) benzaldehyde on the Pd nanoclusters with different sizes. The spectra of free benzyl alcohol and benzaldehyde are shown for comparison. Peaks i–vi correspond to the hydrogen atoms labeled in (a). (f) Schematic mechanism for the size effect of the Pd nanoclusters in catalysis. (g) Reaction selectivity toward benzylidene malononitrile with and without amino groups in the nanoreactors. (h) Benzyl alcohol conversions in eight cycles of the sequential reaction with the Pd-1.3@SiO_2 catalyst and the commercial Pd/C catalyst. The inset shows the HAADF-STEM or TEM images of the catalysts before and after catalysis.

guest molecules involved in the rate-limiting step, i.e., benzyl alcohol and benzaldehyde, on Pd nanoclusters of different sizes by ^{1}H NMR spectroscopy (Fig. 4d, e). Both chemicals were incubated with the Pd-*x*@SiO_2 catalysts, with free molecules removed through repetitive washing using $CDCl_3$ before the ^{1}H NMR analysis. Benzyl alcohol cannot adsorb strongly on Pd nanoclusters and particles of large sizes (i.e., 2.9 and 2.2 nm), as no distinct peaks can be detected in the NMR spectra (Fig. 4d). On Pd nanoclusters of small sizes (i.e., 1.8–0.9 nm), the ^{1}H NMR signals of benzyl alcohol became stronger, indicating stronger adsorption of benzyl alcohol on the Pd nanoclusters. The NMR signals showed a downfield shift and significant line broadening compared with those of pure chemicals. The downfield shift indicates the electron transfer from benzyl alcohol to Pd, leading to a decrease in the electron density around the benzyl alcohol molecules. The significant line broadening can be attributed to the attenuated molecular tumbling of benzyl alcohol molecules on the Pd nanoclusters and hence the reintroduction of dipole-dipole spin interactions [54–57]. Therefore, the ^{1}H NMR signals unambiguously arose from adsorbed benzyl alcohol molecules, not the free ones, which validates the size-dependent adsorption of benzyl alcohol on the Pd nanoclusters. According to the d-band center theory, with the decrease in the size of the Pd nanoclusters, the d-band narrows, and its geometric center shifts upward toward the valence-band minimum, which accounts for the strong adsorption of benzyl alcohol on the Pd nanoclusters [8,58,59]. We attempted to obtain the d-band information experimentally *via* high-resolution valence-band XPS, which turned out to be difficult because XPS, as a surface-sensitive technique, mainly detects the SiO_2 capsule, not the Pd nanoclusters. ^{1}H NMR revealed a distinct trend of the adsorption energy of benzaldehyde on Pd nanoclusters of different sizes (Fig. 4e). Benzaldehyde adsorbs strongly on Pd nanoclusters and particles of large sizes (i.e., 2.9 and 2.2 nm) but weakly on the Pd nanoclusters of small sizes (i.e., 1.8–0.9 nm), which cannot be explained by the d-band center theory. In contrast to benzyl alcohol, which binds to the Pd nanoclusters mainly by σ bonding, benzaldehyde with a C=O group also accepts electrons from Pd, forming π backbonding, which affects the bond strength. The π backbonding depends on the electron density of Pd at the Fermi level. According to the XPS results (Fig. 3a), with the decrease in size, the Pd nanoclusters undergo a distinct

oxidation state transition from metallic to oxide. The decrease in the electron density at the Pd sites may have significantly weakened the π backdonation, leading to the reduced bond strength of benzaldehyde on the Pd nanoclusters [60–62].

Based on these results, the size effect of Pd nanoclusters in catalyzing the benzyl alcohol oxidation reaction (thus the overall sequential reaction) can be rationalized as follows (Fig. 4f): with the decrease in the size of Pd nanoclusters, benzyl alcohol as a reactant adsorbs more strongly on the Pd nanoclusters because of the upward shift of the d-band center, which is favorable for its activation. Meanwhile, benzaldehyde, as a product, adsorbs weakly on the Pd nanoclusters because of the high oxidation state of Pd nanoclusters and thus the weakened electron backdonation, which is favorable for its desorption from the nanocluster surface. Both contribute to the accelerated reaction rates of Pd nanoclusters of small sizes. However, when the size of Pd nanoclusters is too small (0.9 nm), the adsorption of benzyl alcohol becomes too strong, which may significantly poison the Pd surface to yield a slow reaction rate. Consequently, Pd nanoclusters of 1.3 nm show optimal catalytic activity according to the Sabatier principle.

Moreover, the amino groups in the nanoreactors play a critical role in the sequential reaction because the aldehyde produced by alcohol oxidation on Pd nanoclusters migrates to the Pd/–NH_2 interface to initiate the subsequent condensation reaction. Using the Pd-1.3@SiO_2 catalyst, the reaction maintained a high selectivity of no lower than 97% toward benzylidene malononitrile during the entire process (Fig. 4g, red plot). When the amino groups in the catalyst were removed by calcination at 500°C for 2 h, the selectivity of the reaction toward benzylidene malononitrile decreased to <20% (Fig. 4g, blue plot). The capability to modify the environment of noble metal nanoclusters in the nanoreactors makes the strategy appealing in designing complex catalytic systems.

The noble metal nanoclusters are highly stable because they are individually encapsulated in hollow silica nanorods (Fig. 4h). To demonstrate this, the Pd-1.3@SiO_2 catalyst was recovered and applied repeatedly in the sequential reaction. Conversions of benzyl alcohol of no lower than 96% were achieved during eight runs of the catalysis investigated. Furthermore, HAADF-STEM image shows that the structure of the catalyst had been well retained. By contrast, the activity of the Pd/C catalyst rapidly decreased in the first few runs and showed virtually no activity after four runs. The TEM images show that the Pd nanoparticles on the carbon support agglomerated after catalysis, which accounts for the loss of catalytic activity. The high stability of the Pd@SiO_2 catalysts makes them particularly applicable to catalytic applications under harsh conditions.

CONCLUSION

In summary, we have developed an industrially viable impregnation strategy for the synthesis of ligand-free noble metal nanoclusters, which shows combined advantages of simplicity, scalability, and accurate size controllability for catalysis. The introduction of hollow silica nanorods as nanoreactors divides the continuous surface in conventional impregnation synthesis into numerous discrete ones, thus restraining the growth extent of noble metal nanoclusters to ultrasmall sizes. The competitor ions homogenize the adsorption of noble metal ions on the entire surface of the nanoreactor, which eliminates local concentration variations, thereby ensuring only one nucleation event in each nanoreactor. Because of the aforementioned designs, uniform Pd nanoclusters have been successfully prepared, each encapsulated in a hollow silica nanorod, with their size accurately tunable in the range of 0.9–2.9 nm, showing excellent synthetic accuracy at the nanoscale in the impregnation synthesis. Based on the controlled synthesis, we reveal the size-dependent catalytic properties of noble metal nanoclusters in catalysis. Specifically, the Pd nanoclusters of 1.3 nm show higher catalytic activity in the alcohol oxidation-Knoevenagel condensation sequential reaction, compared with Pd nanoclusters of 0.9, 1.8, 2.2, and 2.9 nm, which can be attributed to the unique electronic structure of the nanoclusters for establishing appropriate interactions with the reactants and intermediates, according to the Sabatier principle. In particular, the size effect of the Pd nanoclusters is demonstrated to push the benzyl alcohol oxidation activity to a high level, hinting at the capability of this strategy for catalytic screening toward unprecedented catalytic activities. Moreover, the nanoreactors endow the noble metal nanoclusters with high stability against agglomeration during the catalysis. This strategy is general as verified by its applicability to other noble metal nanoclusters, e.g., Au, Pt, and Ru. We believe this study opens new opportunities for rationally designing and optimizing highly efficient noble metal catalysts, fundamentally understanding their size effect, and bringing efficient laboratory-quality noble metal catalysts to large-scale applications.

Received 31 July 2022; accepted 8 September 2022; published online 30 November 2022

1 Yan J, Teo BK, Zheng N. Surface chemistry of atomically precise coinage-metal nanoclusters: From structural control to surface reactivity and catalysis. Acc Chem Res, 2018, 51: 3084–3093
2 Gao C, Lyu F, Yin Y. Encapsulated metal nanoparticles for catalysis. Chem Rev, 2021, 121: 834–881
3 Chen X, Peng M, Cai X, *et al.* Regulating coordination number in atomically dispersed Pt species on defect-rich graphene for *n*-butane dehydrogenation reaction. Nat Commun, 2021, 12: 2664
4 Wang L, Diao J, Peng M, *et al.* Cooperative sites in fully exposed Pd clusters for low-temperature direct dehydrogenation reaction. ACS Catal, 2021, 11: 11469–11477
5 Liu M, Liu M, Wang X, *et al.* Quantum-dot-derived catalysts for CO_2 reduction reaction. Joule, 2019, 3: 1703–1718
6 Kuhn JN, Huang W, Tsung CK, *et al.* Structure sensitivity of carbon-nitrogen ring opening: Impact of platinum particle size from below 1 to 5 nm upon pyrrole hydrogenation product selectivity over monodisperse platinum nanoparticles loaded onto mesoporous silica. J Am Chem Soc, 2008, 130: 14026–14027
7 Yamamoto K, Imaoka T, Chun WJ, *et al.* Size-specific catalytic activity of platinum clusters enhances oxygen reduction reactions. Nat Chem, 2009, 1: 397–402
8 Bai L, Wang X, Chen Q, *et al.* Explaining the size dependence in platinum-nanoparticle-catalyzed hydrogenation reactions. Angew Chem Int Ed, 2016, 55: 15656–15661
9 Wang H, Gu XK, Zheng X, *et al.* Disentangling the size-dependent geometric and electronic effects of palladium nanocatalysts beyond selectivity. Sci Adv, 2019, 5: eaat6413
10 Guan Q, Zhu C, Lin Y, *et al.* Bimetallic monolayer catalyst breaks the activity-selectivity trade-off on metal particle size for efficient chemoselective hydrogenations. Nat Catal, 2021, 4: 840–849
11 Mistry H, Reske R, Zeng Z, *et al.* Exceptional size-dependent activity enhancement in the electroreduction of CO_2 over Au nanoparticles. J Am Chem Soc, 2014, 136: 16473–16476
12 Liu Y, Tsunoyama H, Akita T, *et al.* Aerobic oxidation of cyclohexane catalyzed by size-controlled Au clusters on hydroxyapatite: Size effect in

the sub-2 nm regime. ACS Catal, 2010, 1: 2–6
13 Li G, Jin R. Gold nanocluster-catalyzed semihydrogenation: A unique activation pathway for terminal alkynes. J Am Chem Soc, 2014, 136: 11347–11354
14 Li G, Jiang D, Kumar S, *et al.* Size dependence of atomically precise gold nanoclusters in chemoselective hydrogenation and active site structure. ACS Catal, 2014, 4: 2463–2469
15 Bai L, Zhang S, Chen Q, *et al.* Synthesis of ultrasmall platinum nanoparticles on polymer nanoshells for size-dependent catalytic oxidation reactions. ACS Appl Mater Interfaces, 2017, 9: 9710–9717
16 Zhao H, Yao S, Zhang M, *et al.* Ultra-small platinum nanoparticles encapsulated in sub-50 nm hollow titania nanospheres for low-temperature water-gas shift reaction. ACS Appl Mater Interfaces, 2018, 10: 36954–36960
17 Yao Q, Chen T, Yuan X, *et al.* Toward total synthesis of thiolate-protected metal nanoclusters. Acc Chem Res, 2018, 51: 1338–1348
18 Chakraborty I, Pradeep T. Atomically precise clusters of noble metals: Emerging link between atoms and nanoparticles. Chem Rev, 2017, 117: 8208–8271
19 Jin R, Zeng C, Zhou M, *et al.* Atomically precise colloidal metal nanoclusters and nanoparticles: Fundamentals and opportunities. Chem Rev, 2016, 116: 10346–10413
20 Yamamoto K, Imaoka T, Tanabe M, *et al.* New horizon of nanoparticle and cluster catalysis with dendrimers. Chem Rev, 2019, 120: 1397–1437
21 Ye R, Zhukhovitskiy AV, Kazantsev RV, *et al.* Supported Au nanoparticles with *N*-heterocyclic carbene ligands as active and stable heterogeneous catalysts for lactonization. J Am Chem Soc, 2018, 140: 4144–4149
22 Deraedt C, Ye R, Ralston WT, *et al.* Dendrimer-stabilized metal nanoparticles as efficient catalysts for reversible dehydrogenation/hydrogenation of *N*-heterocycles. J Am Chem Soc, 2017, 139: 18084–18092
23 Sun N, Wang C, Wang H, *et al.* Multifunctional tubular organic cage-supported ultrafine palladium nanoparticles for sequential catalysis. Angew Chem Int Ed, 2019, 58: 18011–18016
24 Yang X, Sun JK, Kitta M, *et al.* Encapsulating highly catalytically active metal nanoclusters inside porous organic cages. Nat Catal, 2018, 1: 214–220
25 Fang Y, Xiao Z, Li J, *et al.* Formation of a highly reactive cobalt nanocluster crystal within a highly negatively charged porous coordination cage. Angew Chem Int Ed, 2018, 57: 5283–5287
26 Mondal B, Acharyya K, Howlader P, *et al.* Molecular cage impregnated palladium nanoparticles: Efficient, additive-free heterogeneous catalysts for cyanation of aryl halides. J Am Chem Soc, 2016, 138: 1709–1716
27 McCaffrey R, Long H, Jin Y, *et al.* Template synthesis of gold nanoparticles with an organic molecular cage. J Am Chem Soc, 2014, 136: 1782–1785
28 Zhao H, Wang D, Gao C, *et al.* Ultrafine platinum/iron oxide nanoconjugates confined in silica nanoshells for highly durable catalytic oxidation. J Mater Chem A, 2016, 4: 1366–1372
29 Zhang T, Zhao H, He S, *et al.* Unconventional route to encapsulated ultrasmall gold nanoparticles for high-temperature catalysis. ACS Nano, 2014, 8: 7297–7304
30 Lu L, Zou S, Fang B. The critical impacts of ligands on heterogeneous nanocatalysis: A review. ACS Catal, 2021, 11: 6020–6058
31 Bryant K, West CW, Saunders SR. Impacts of calcination on surface-clean supported nanoparticle catalysts. Appl Catal A-Gen, 2019, 579: 58–64
32 Donoeva B, de Jongh PE. Colloidal Au catalyst preparation: Selective removal of polyvinylpyrrolidone from active Au sites. ChemCatChem, 2018, 10: 989–997
33 Fan Q, Liu K, Liu Z, *et al.* A ligand-exchange route to nobel metal nanocrystals with a clean surface for enhanced optical and catalytic properties. Part Part Syst Charact, 2017, 34: 1700075
34 Geus JW, van Dillen AJ. Supported catalysts. In: Ertl G, Knözinger H, Schüth F, Weitkamp J (Eds.). Handbook of Heterogeneous Catalysis. Weinheim: Wiley-VCH, 2008. 428–655
35 Munnik P, de Jongh PE, de Jong KP. Recent developments in the synthesis of supported catalysts. Chem Rev, 2015, 115: 6687–6718
36 Wang N, Sun Q, Zhang T, *et al.* Impregnating subnanometer metallic nanocatalysts into self-pillared zeolite nanosheets. J Am Chem Soc, 2021, 143: 6905–6914
37 Kou Y, Sun LB. Size regulation of platinum nanoparticles by using confined spaces for the low-temperature oxidation of ethylene. Inorg Chem, 2018, 57: 1645–1650
38 Shi LY, Li YX, Xue DM, *et al.* Facile fabrication of small-sized palladium nanoparticles in nanoconfined spaces for low-temperature CO oxidation. Ind Eng Chem Res, 2020, 59: 19145–19152
39 Gao C, Lu Z, Yin Y. Gram-scale synthesis of silica nanotubes with controlled aspect ratios by templating of nickel-hydrazine complex nanorods. Langmuir, 2011, 27: 12201–12208
40 Gao C, Zhang Q, Lu Z, *et al.* Templated synthesis of metal nanorods in silica nanotubes. J Am Chem Soc, 2011, 133: 19706–19709
41 Haynes WM. CRC Handbook of Chemistry and Physics. Boca Raton: CRC Press, 2017
42 Wang H, Wang Y, Zhu Z, *et al.* Influence of size-induced oxidation state of platinum nanoparticles on selectivity and activity in catalytic methanol oxidation in the gas phase. Nano Lett, 2013, 13: 2976–2979
43 Sun Y, Zhuang L, Lu J, *et al.* Collapse in crystalline structure and decline in catalytic activity of Pt nanoparticles on reducing particle size to 1 nm. J Am Chem Soc, 2007, 129: 15465–15467
44 Hu Y, Zhang Q, Goebl J, *et al.* Control over the permeation of silica nanoshells by surface-protected etching with water. Phys Chem Chem Phys, 2010, 12: 11836–11842
45 Li YA, Yang S, Liu QK, *et al.* Pd(0)@UiO-68-AP: Chelation-directed bifunctional heterogeneous catalyst for stepwise organic transformations. Chem Commun, 2016, 52: 6517–6520
46 Cao CC, Chen CX, Wei ZW, *et al.* Catalysis through dynamic spacer installation of multivariate functionalities in metal-organic frameworks. J Am Chem Soc, 2019, 141: 2589–2593
47 Sun Q, Aguila B, Ma S. A bifunctional covalent organic framework as an efficient platform for cascade catalysis. Mater Chem Front, 2017, 1: 1310–1316
48 Feng D, Dong Y, Zhang L, *et al.* Holey lamellar high-entropy oxide as an ultra-high-activity heterogeneous catalyst for solvent-free aerobic oxidation of benzyl alcohol. Angew Chem Int Ed, 2020, 59: 19503–19509
49 Lackmann A, Mahr C, Schowalter M, *et al.* A comparative study of alcohol oxidation over nanoporous gold in gas and liquid phase. J Catal, 2017, 353: 99–106
50 Meher S, Rana RK. A rational design of a Pd-based catalyst with a metal-metal oxide interface influencing molecular oxygen in the aerobic oxidation of alcohols. Green Chem, 2019, 21: 2494–2503
51 Wei Q, Yu C, Song X, *et al.* Recognition of water-induced effects toward enhanced interaction between catalyst and reactant in alcohol oxidation. J Am Chem Soc, 2021, 143: 6071–6078
52 Xin P, Li J, Xiong Y, *et al.* Revealing the active species for aerobic alcohol oxidation by using uniform supported palladium catalysts. Angew Chem Int Ed, 2018, 57: 4642–4646
53 Zhu L, Lin Y, Liu K, *et al.* Tuning the intermediate reaction barriers by a CuPd catalyst to improve the selectivity of CO_2 electroreduction to C_2 products. Chin J Catal, 2021, 42: 1500–1508
54 Hostetler MJ, Wingate JE, Zhong CJ, *et al.* Alkanethiolate gold cluster molecules with core diameters from 1.5 to 5.2 nm: Core and monolayer properties as a function of core size. Langmuir, 1998, 14: 17–30
55 Marbella LE, Andolina CM, Smith AM, *et al.* Gold-cobalt nanoparticle alloys exhibiting tunable compositions, near-infrared emission, and high T_2 relaxivity. Adv Funct Mater, 2014, 24: 6532–6539
56 Marbella LE, Millstone JE. NMR techniques for noble metal nanoparticles. Chem Mater, 2015, 27: 2721–2739
57 Terrill RH, Postlethwaite TA, Chen C, *et al.* Monolayers in three dimensions: NMR, SAXS, thermal, and electron hopping studies of alkanethiol stabilized gold clusters. J Am Chem Soc, 1995, 117: 12537–12548
58 Nørskov JK, Abild-Pedersen F, Studt F, *et al.* Density functional theory in surface chemistry and catalysis. Proc Natl Acad Sci USA, 2011, 108: 937–943
59 Nørskov JK, Bligaard T, Rossmeisl J, *et al.* Towards the computational design of solid catalysts. Nat Chem, 2009, 1: 37–46

60 Kalhara Gunasooriya GTK, Saeys M. CO adsorption site preference on platinum: Charge is the essence. ACS Catal, 2018, 8: 3770–3774
61 Xu W, Zhang M, Ma C, *et al.* Amorphous $NiSb_2O_{6-x}$ nanofiber: A *d*-/*p*-block Janus electrocatalyst toward efficient NH_3 synthesis through boosted N_2 adsorption and activation. Appl Catal B-Environ, 2022, 308: 121225
62 Lin G, Ju Q, Guo X, *et al.* Intrinsic electron localization of metastable MoS_2 boosts electrocatalytic nitrogen reduction to ammonia. Adv Mater, 2021, 33: 2007509

Acknowledgements This work was supported by the National Natural Science Foundation of China (22071191), the Key Research and Development Projects of Shaanxi Province (2021GXLH-Z-022), the Fundamental Research Funds for the Central Universities, and the Key Scientific and Technological Innovation Team of Shaanxi Province (2020TD-001). Liu K acknowledges China Postdoctoral Science Foundation (2019TQ0249) and the Natural Science Basic Research Plan in Shaanxi Province (2022JQ-100). The authors thank the Instrument Analysis Center of Xi'an Jiaotong University for the assistance with HRTEM and XPS measurements.

Author contributions Gao C conceived the idea and supervised the project. Wen Z conducted the synthesis, characterization, and catalysis. Zhang S, Liu Z, Zhang Z, Qiao Z, and Liu K assisted in materials characterizations. Wen Z and Gao C wrote the manuscript. All authors discussed the results and revised the manuscript.

Conflict of interest The authors declare that they have no conflict of interest.

Supplementary information Experimental details and supporting data are available in the online version of the paper.

Zhibin Wen received his BS degree from the Northwest A&F University in 2016 and then obtained his MS degree from the Southwest University in 2019. He is currently a PhD candidate at the Frontier Institute of Science and Technology, Xi'an Jiaotong University. His research interest is the synthesis of noble metal nanoclusters for catalysis.

Chuanbo Gao received his PhD degree in applied chemistry in 2009 from Shanghai Jiao Tong University and carried out his postdoctoral research at the University of California, Riverside. Since 2012 he has been a professor at the Frontier Institute of Science and Technology, Xi'an Jiaotong University. His research interest is the precision synthesis of noble metal-based nanomaterials for catalysis and energy conversion.

浸渍法制备尺寸均一可调的贵金属纳米团簇及其尺寸依赖的催化性质

文智斌, 张树蒙, 刘钊钧, 张志学, 乔准, 刘凯, 高传博*

摘要 贵金属纳米团簇作为原子和纳米颗粒的中间形态, 表现出特殊的电子结构和优异的催化性能. 目前, 这类纳米团簇通常通过湿化学法合成, 其表面常被配体所钝化, 而通过浸渍法合成的贵金属纳米团簇通常表现出较宽的尺寸分布. 本研究以钯为例, 发展了基于浸渍法精准合成尺寸介于0.9和2.9 nm、无表面配体的贵金属纳米团簇的新范式. 该方法关键在于采用二氧化硅纳米胶囊为纳米反应器并引入非贵金属竞争吸附离子, 从而达到严格控制贵金属纳米团簇成核和生长的目的, 因此具有操作便利、合成可放大及纳米团簇尺寸精准可调等优势. 钯纳米团簇在醇氧化-Knoevenagel缩合连续反应中表现出显著的尺寸效应, 其中1.3 nm的钯纳米团簇具有最优的催化活性. 这一新颖的合成策略为贵金属纳米团簇型催化剂的开发提供了新思路, 为实验室级高品质纳米团簇催化剂的规模应用提供了可行方案.

